AMERICAN SOCIETY FOR MICROBIOLOGY | mSystems®

RESEARCH ARTICLE
Ecological and Evolutionary Science

Quantification of Lysogeny Caused by Phage Coinfections in Microbial Communities from Biophysical Principles

Antoni Luque,[a,b,c] Cynthia B. Silveira[d]

[a]Department of Mathematics and Statistics, San Diego State University, San Diego, California, USA
[b]Viral Information Institute, San Diego State University, San Diego, California, USA
[c]Computational Science Research Center, San Diego State University, San Diego, California, USA
[d]Department of Biology, University of Miami, Coral Gables, Florida, USA

Both authors contributed equally to this work. Author order was determined alphabetically by last name.

ABSTRACT Temperate phages can associate with their bacterial host to form a lysogen, often modifying the phenotype of the host. Lysogens are dominant in the microbially dense environment of the mammalian gut. This observation contrasts with the long-standing hypothesis of lysogeny being favored at low microbial densities, such as in oligotrophic marine environments. Here, we hypothesized that phage coinfections—a well-understood molecular mechanism of lysogenization—increase at high microbial abundances. To test this hypothesis, we developed a biophysical model of coinfection for marine and gut microbiomes. The model stochastically sampled ranges of phage and bacterial concentrations, adsorption rates, lysogenic commitment times, and community diversity from each environment. In 90% of the sampled marine communities, less than 10% of the bacteria were predicted to be lysogenized via coinfection. In contrast, 25% of the sampled gut communities displayed more than 25% of lysogenization. The probability of lysogenization in the gut was a consequence of the higher densities and higher adsorption rates. These results suggest that, on average, coinfections can form two trillion lysogens in the human gut every day. In marine microbiomes, which were characterized by lower densities and phage adsorption rates, lysogeny via coinfection was still possible for communities with long lysogenic commitment times. Our study indicates that different physical factors causing coinfections can reconcile the traditional view of lysogeny at poor host growth (long commitment times) and the recent Piggyback-the-Winner framework proposing that lysogeny is favored in rich environments (high densities and adsorption rates).

IMPORTANCE The association of temperate phages and bacterial hosts during lysogeny manipulates microbial dynamics from the oceans to the human gut. Lysogeny is well studied in laboratory models, but its environmental drivers remain unclear. Here, we quantified the probability of lysogenization caused by phage coinfections, a well-known trigger of lysogeny, in marine and gut microbial environments. Coinfections were quantified by developing a biophysical model that incorporated the traits of viral and bacterial communities. Lysogenization via coinfection was more frequent in highly productive environments like the gut, due to higher microbial densities and higher phage adsorption rates. At low cell densities, lysogenization occurred in bacteria with long duplication times. These results bridge the molecular understanding of lysogeny with the ecology of complex microbial communities.

KEYWORDS stochastic biophysical model, lysogeny, microbial abundance, multiplicity of infection, adsorption rates, commitment time

Citation Luque A, Silveira CB. 2020. Quantification of lysogeny caused by phage coinfections in microbial communities from biophysical principles. mSystems 5:e00353-20. https://doi.org/10.1128/mSystems.00353-20.

Editor Seth Bordenstein, Vanderbilt University

Address correspondence to Antoni Luque, aluque@sdsu.edu, or Cynthia B. Silveira, cynthiasilveira@miami.edu.

Received 21 April 2020
Accepted 25 August 2020
Published 15 September 2020

Temperate phages can integrate into their host's genome as a prophage or persist as extrachromosomal elements forming a lysogen. Half of the genomes that have been sequenced from bacterial isolates contain prophages (1–3). Most lysogens display changes in phenotypes, such as protection against other phage infections and additional metabolic functions (4–6). Despite lysogeny's profound impacts on the structure and functioning of microbial communities, its environmental drivers remain unclear.

Currently, the best proxies to estimate the frequency of lysogeny in microbial communities are the distributions of integrases, excisionases, lysis repressors, and sequences with high similarity with reference prophages (7, 8). The abundance of these markers in metagenomic data indicates that microbially dense environments, such as the mammalian gut, are dominated by temperate phages and bacterial lysogens (9–14). The high frequency of lysogeny in the gut can be explained by the Piggyback-the-Winner (PtW) framework, which proposes that the phenotypic advantages of lysogeny are favored at high host abundances (15–17).

Compared to animal-associated microbial communities, aquatic marine ecosystems have much weaker lysogenic signatures (7, 15). Genomic analyses have indicated that lysogeny is frequent in deep oligotrophic waters (18–20). In these environments where bacterial abundances are low, ranging from 10^4 to 10^5 cells per ml, 98% of the temperate viral sequences observed in the cellular metagenomes are also found in the virome (7). The increase in lysogeny in marine ecosystems with low productivity has been historically hypothesized to serve as a low-density refugium for phages during poor host growth (21). However, highly productive marine ecosystems where abundances of bacteria rise above 10^6 cells per ml also increase their lysogenic signatures, following the PtW framework (15). This is consistent with the observation that high intrinsic growth rates are the most important predictor of the frequency of prophages in bacteria with complete genomes sequenced (1, 22). Growth rates alone cannot explain the prevalence of lysogeny under both high- and low-productivity conditions, suggesting that density-dependent factors might play a role.

Phage coinfections promote lysogenization in model phage and bacteria under both poor and rich growth conditions (23–25). In lambda phage, the percentage of lysogenized cells increases from 0.1% to close to 100% when the multiplicity of infection (MOI) increases from 0.05 to 100 phages per bacteria (26–30). Coinfections increase the expression of the lambda repressors of the lytic pathway and activate a cascade of genes responsible for phage integration (31–33). The response of lysogeny to coinfection seems to represent a widespread strategy among temperate phage populations. Most temperate phages encode a repressor system functionally similar to lambda's cro/cI (34). For example, phage P22, which displays only 13% genomic similarity with lambda, encodes the same repressor system (35). Even phages such as Mu and Epsilon15, with completely distinct molecular mechanisms for the control of lysogeny, also increase lysogeny at higher rates of coinfection (36). Yet, the extent to which coinfections occur in complex microbial communities, and their impact on lysogeny, has not been quantified.

After its first introduction, the term MOI became known in the field as the initial ratio of phage particles (P_0) to bacterial cells (B_0) added to an experiment ($MOI = P_0/B_0$). This definition of MOI, however, does not necessarily capture the effective number of coinfections, which also depends on the chances of encounter between the phage and the host (37). A recent stochastic model shows that at the single-cell level, the average number of coinfections is primarily determined by the phage concentrations and phage decision times (38). Because highly productive environments have higher phage concentrations, here we hypothesize that the prevalence of lysogeny in these environments is a consequence of an increase in coinfections.

To test this hypothesis, a biophysical model was derived to incorporate the physical traits that determine phage (co)infection (COI) and its associated probability of lysogeny. The model was simulated for a range of phage and bacterial abundances, community diversity, adsorption rates, and lysogenic commitment times from marine and mammalian gut communities. The availability of large amounts of public data from

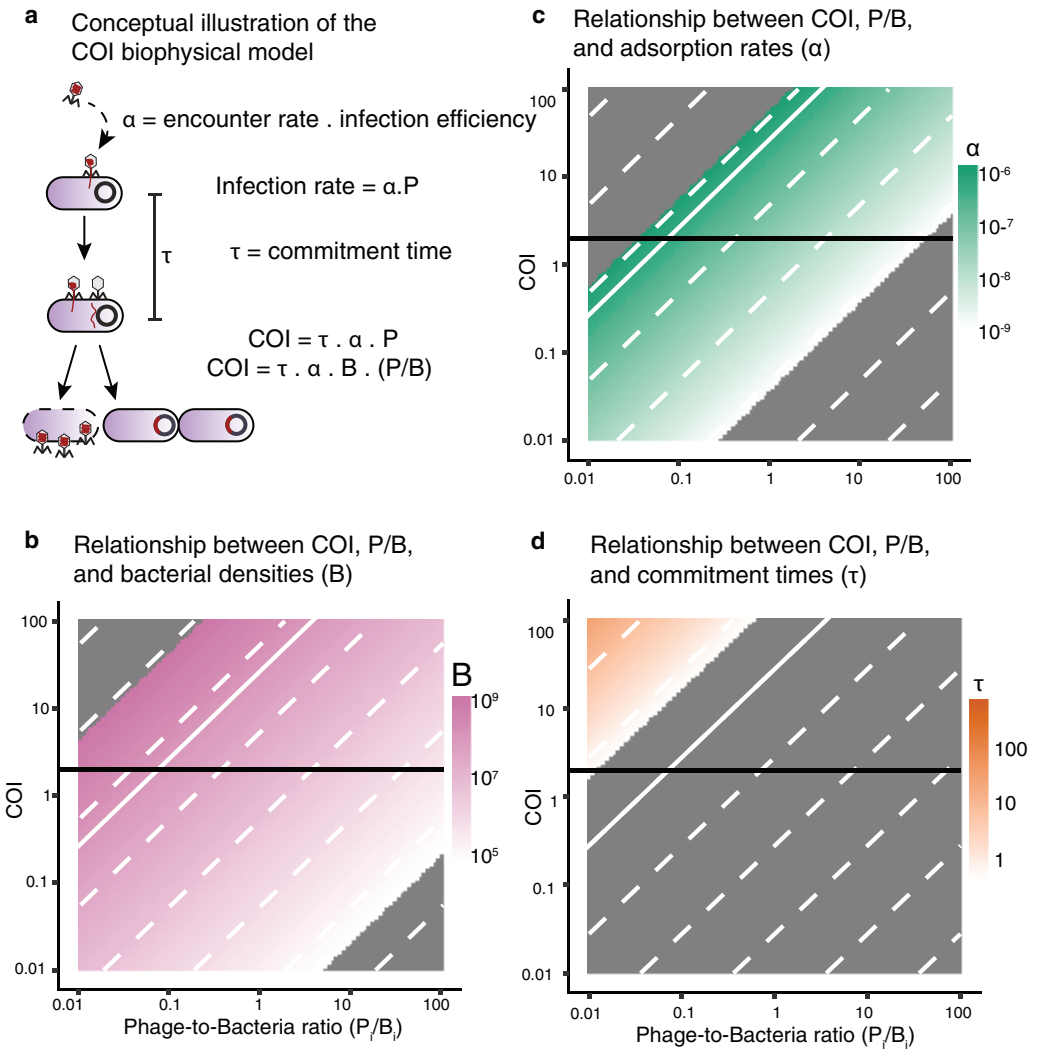

FIG 1 Relationship between number of (co)infections and phage-to-bacterium ratios. (a) Illustration of the derivation and parameter description for the biophysical (co)infection (COI) model, equation 1. COI was defined as the average number of phages infecting a cell within the commitment time (τ). COI = 1 means one phage infection. COI = 2 means two phage infections. (b to d) Relationship between COI and phage-to-bacterium ratios as a function of bacterial abundances (b), adsorption rates (c), and lysogenic commitment times (d). Panels b to d are contour plots of the quantitative outputs of the dependencies from equation 1. The color gradients cover the environmental ranges of values for each of these parameters: bacterial concentrations (pink), adsorption rates (green), and lysogenic commitment times (orange). (b to d) The dashed white lines indicate constant values of the parameters in the gradient scale. The gray areas correspond to values beyond the environmental ranges of bacterial concentrations, adsorption rates, and commitment times obtained from the meta-analysis of marine and gut ecosystems. The horizontal black line indicates COI = 2, that is, two average phage infections within the commitment time (τ). The solid white line indicates the median values for the bacterial concentration (B_0), adsorption rates (α_0), and lysogenic commitment time (τ_0) for lambda in laboratory experiments.

these two ecosystems allowed us to test the hypothesis across a wide range of microbial densities.

RESULTS

Relationship between COI and phage-to-bacterium ratios. The model introduced in equation 1 was reexpressed to estimate the average number of phage (co)infections (COI) in terms of the phage-to-bacterium ratios (P_i/B_i) for a single phage-host pair (Fig. 1a). The phage-to-bacterium ratio (P_i/B_i) was used as a proxy for the operational multiplicity of infection (MOI = P_0/B_0) widely used in the phage field. The bacterial densities, adsorption rates, and commitment times were plotted as a function of COI and P_i/B_i (Fig. 1b to d). To illustrate the relationship of COI with different

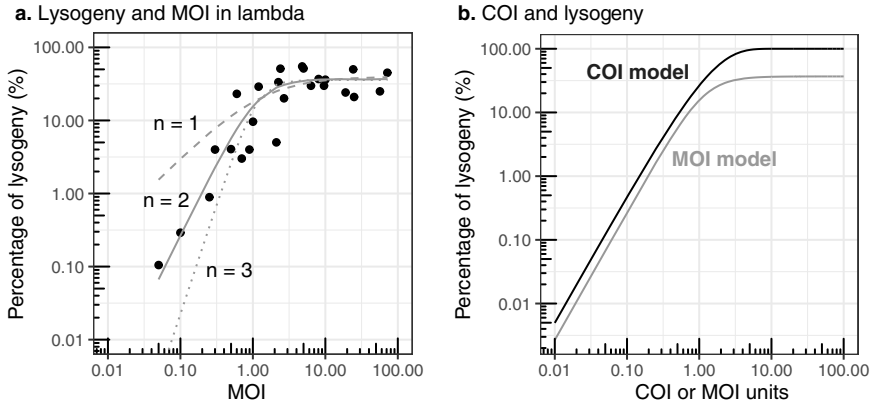

FIG 2 Comparison of percentage of lysogeny for lambda MOI and COI model. (a) Relationship between the percentage of lysogeny and MOI (initial phage-to-bacterium ratio) in lambda-*E. coli* experiments (28, 29). The lines correspond to fitted Hill-Langmuir cooperation models of order $n = 1$ (dashed), $n = 2$ (solid), and $n = 3$ (dotted). (b) Percentage of lysogeny estimated from the coinfection probability model as a function of COI, equation 2 (solid black line). Hill-Langmuir model of order $n = 2$ from panel a as a function of MOI (solid gray line).

physical parameters, only one value was varied at a time covering typical environmental ranges (see meta-analysis section for environmental ranges). COI was higher for higher bacterial concentrations (Fig. 1b), phage adsorption rate constants (Fig. 1c), and lysogenic commitment times (Fig. 1d). For the typical adsorption rate and commitment time of lambda, the model showed that an average of two or more phage infections (COI $\geqslant$ 2) was unlikely to occur at bacterial densities below 10^6 cells/ml, even for phage-to-bacterium ratios above 10 (bottom right values in Fig. 1b). Due to the high adsorption rate of lambda, the average number of coinfections generated per phage-to-bacterium ratio was near the upper range of environmental values (Fig. 1c). Due to the short lysogenic commitment time of lambda, the average coinfections per phage-to-bacterium ratio unit were below the environmental values (Fig. 1d). These results show that as one departs from ideal experimental conditions, the proxy for MOI did not capture the average number of coinfections.

The probability of lysogeny as a function of average coinfections (COI) was compared with lambda-*Escherichia coli* MOI experiments. The percentage of lysogenized cells increased as a function of MOI and was best described by a sigmoidal Hill-Langmuir equation of order $n = 2$, compared to orders $n = 1$ and $n = 3$ (Fig. 2a). This equation implied that two phages cooperated in producing lysogeny, in agreement with single-molecule experiments (25). This empirical model was functionally similar to the predicted probability of lysogeny from the average coinfection Poisson model, equation 2, which assumed that at least two infections were necessary to produce lysogeny (Fig. 2b). The MOI and COI values were similar. The discrepancy between the maximum percentages of lysogeny for the MOI and COI models was due to the fact that the COI model was a function of the initial phage-to-bacterium ratio and did not account for the rapid removal of phage particles due to cell adsorption in the course of the experiments. The MOI-COI equivalence in lambda-*E. coli* experiments was due to the fact that the original MOI experiments were set up to capture the number of coinfections, which was only possible for those specific growth conditions (Fig. 1).

Meta-analysis of COI physical parameters from marine and animal ecosystems. To apply the biophysical COI model to microbial communities and estimate lysogeny generated by phage coinfections, the ranges of phage adsorption rate constants, lysogenic commitment times, and phage-bacterium pair abundances were determined for marine and animal ecosystems. The range of adsorption rates was $7.2 \cdot 10^{-10}$ to $3.7 \cdot 10^{-7}$ ml/h for marine phages infecting *Prochlorococcus* sp., *Roseobacter* sp., *Pseudoalteromonas* sp., *Synechococcus* sp., and *Vibrio* sp. (Fig. 3a). The range of adsorption

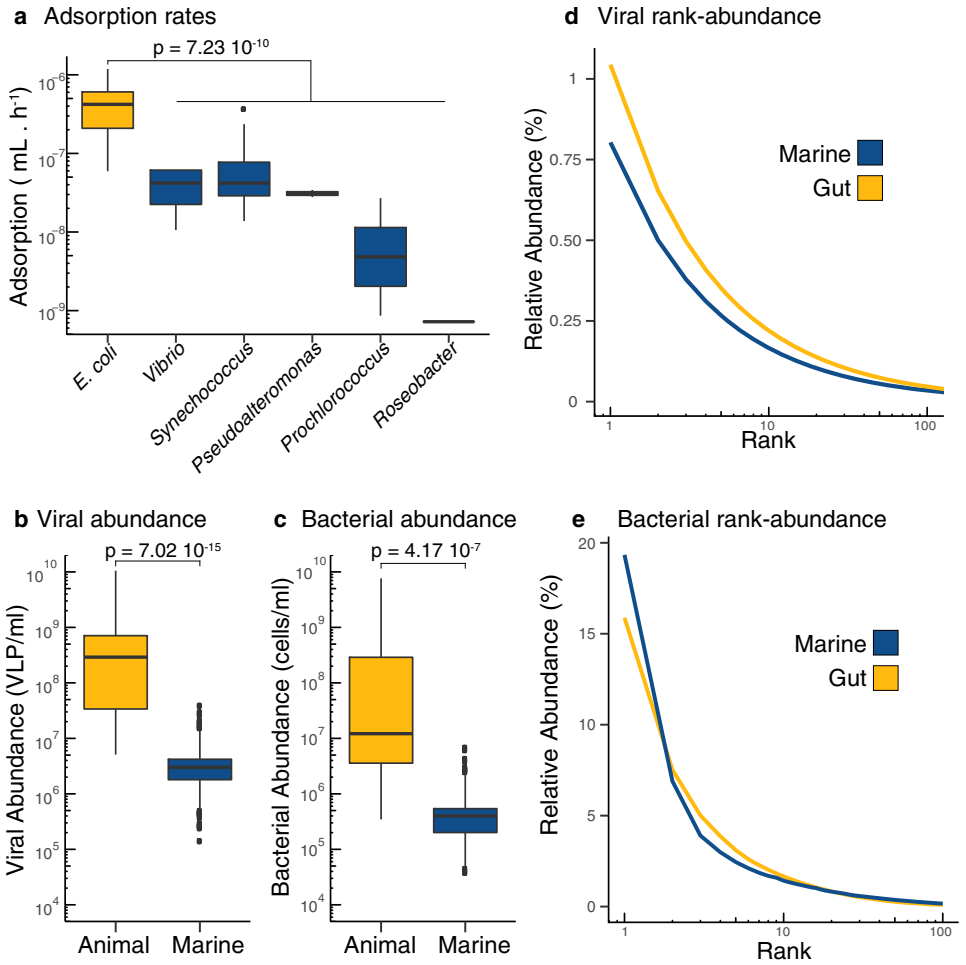

FIG 3 Meta-analysis of COI parameters in marine and animal microbiomes. (a) Adsorption rates from single phage-host pairs of bacterial hosts derived from the mammalian gut (yellow) and marine environments (blue). The same color coding applies to all panels. (b and c) Viral abundances (b) and bacterial abundances (c) per ml in animal-associated and marine environments. (d) Rank-abundance curve displaying the top 100 ranks of phage genotypes identified in metagenomic data from human gut and marine samples. (e) Rank-abundance curve displaying the top 100 ranks of bacterial genotypes identified in metagenomic data from human gut and marine samples. The references for each original study, and the values for each data point are provided as Data Sets S1 to S5.

rates was $5.9 \cdot 10^{-8}$ to $1.2 \cdot 10^{-6}$ ml/h for gut phages infecting *E. coli*. The median adsorption rate for gut phages was 1 order of magnitude higher ($4.2 \cdot 10^{-7}$ ml/h) than the median for marine phages ($3.4 \cdot 10^{-8}$ ml/h [Fig. 3a], and *t* test $P = 7.23 \cdot 10^{-10}$). Lysogenic commitment times were longer in marine communities, 11 to 808 h, than in the mammalian gut, 2.74 to 7.27 h. This was a consequence of the long duplication times of marine communities in their natural environment. The phage and bacterium pair abundances were determined by combining the total and relative abundances of phage and bacteria in each ecosystem. Phage abundances were $1.4 \cdot 10^5$ to $3.7 \cdot 10^7$ phages/ml (marine) and $5.1 \cdot 10^6$ to $1.1 \cdot 10^{10}$ phages/ml (animal) (Fig. 3b). Bacterial abundances ranged from $3.8 \cdot 10^4$ to $6.8 \cdot 10^6$ cells/ml (marine) and from $3.5 \cdot 10^5$ to $7.7 \cdot 10^9$ cells/ml (animal) (Fig. 3c). The total abundances were at least 2 orders of magnitude higher in animal-associated mucosa than in the free-living communities of surface marine environments (*t* test $P = 7.02 \cdot 10^{-15}$ for phage [Fig. 3b], and *P* value $= 4.17 \cdot 10^{-7}$ for bacteria [Fig. 3c]). The most abundant phage genotype (P_1) in marine environments comprised only 0.8% of the total phage community, while in the gut, the dominant phage comprised just over 1% of the community (Fig. 3d). In the bacterial community, this pattern was inverted, with the dominant bacterial species (B_1) reaching 19% in marine environments, but only 15% in the gut (Fig. 3e).

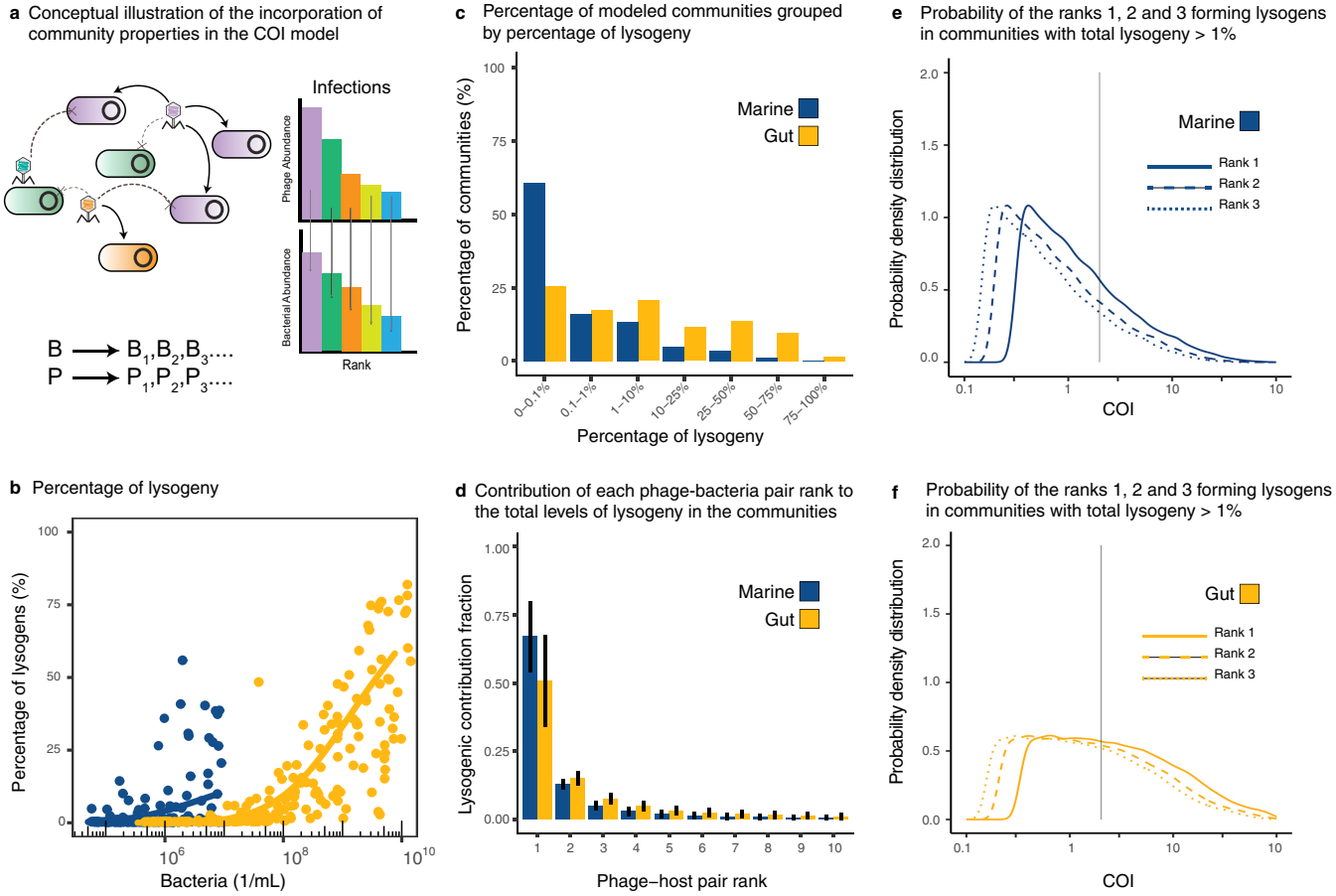

FIG 4 Lysogeny caused by coinfections in communities. (a) Conceptual figure describing the implementation of the biophysical COI model with a stochastic sampling of community parameters. Each phage P_i infected each bacterium B_i according to their ranks in the community. The chances of encounter decreased with phage-host rank as a function of their absolute abundances in the community. (b) Percentage of lysogenic cells in the bacterial community predicted to be formed through phage coinfections as a function of the total bacterial density. The data points are a subsample of 200 stochastic models out of 100,000 sampled models for each ecosystem. The solid lines represent generalized additive models (GAM) fitted to the full data set for marine (blue) and gut (yellow) ecosystems. (c) Percentage of sampled communities displaying different ranges of lysogeny. (d) Average contribution (with error bars corresponding to SD) from the top phage-bacterium pair ranks to the lysogenic pool. (e and f) Probability distributions of average phage coinfections (COI) for the top ranks in communities with lysogeny above 1% for marine and gut ecosystems. The vertical line indicates COI = 2, that is, the average of two phage infections within the commitment time.

Lysogeny by coinfection in microbial communities. The community model assumed a direct phage-host network, where each phage rank infected the same rank in the bacterial community, that is, P_i infected B_i (Fig. 4a). The biophysical COI model quantified the percentage of lysogeny generated by phage coinfections for each pair by stochastically sampling the parameter ranges from the meta-analysis of marine and gut ecosystems. The percentage of lysogeny caused by coinfections increased with total bacterial density (Fig. 4b and Fig. S1). Lysogeny was more frequent in the gut, where 25% of the simulated communities displayed at least 25% of bacteria becoming lysogens by coinfection (Fig. 4c, Table 1, and Table S1). The median percentage of lysogeny in these communities was 47.8%. Given the median bacterial abundances

TABLE 1 Summary statistics for gut communities with lysogeny ≥25%[a]

Feature	Unit	Min	1st Qu	Median	Mean	3rd Qu	Max
Bacterial concentration	Cells/ml	$5.6 \cdot 10^6$	$6.8 \cdot 10^8$	$1.8 \cdot 10^9$	$2.4 \cdot 10^9$	$3.9 \cdot 10^9$	$7.6 \cdot 10^9$
Phage concentration	Phages/ml	$2.0 \cdot 10^8$	$8.0 \cdot 10^8$	$1.3 \cdot 10^9$	$1.9 \cdot 10^9$	$2.2 \cdot 10^9$	$1.1 \cdot 10^{10}$
Phage adsorption rate	ml/h	$5.9 \cdot 10^{-9}$	$1.3 \cdot 10^{-7}$	$2.6 \cdot 10^{-7}$	$3.7 \cdot 10^{-7}$	$5.6 \cdot 10^{-7}$	$1.2 \cdot 10^{-6}$
Lysogenic commitment time	h	0.55	0.74	0.95	0.97	1.19	1.45

[a]Abbreviations: Min, minimum; Qu, Quartile; Max, maximum.

TABLE 2 Summary statistics for marine communities with lysogeny ≥10%[a]

Feature	Unit	Min	1st Qu	Median	Mean	3rd Qu	Max
Bacterial concentration	Cells/ml	$3.8 \cdot 10^4$	$7.9 \cdot 10^5$	$2.0 \cdot 10^6$	$2.5 \cdot 10^6$	$3.9 \cdot 10^6$	$6.7 \cdot 10^6$
Phage concentration	Phages/ml	$6.2 \cdot 10^5$	$6.3 \cdot 10^6$	$1.3 \cdot 10^7$	$1.6 \cdot 10^7$	$2.5 \cdot 10^7$	$3.9 \cdot 10^7$
Phage adsorption rate	ml/h	$6.2 \cdot 10^{-9}$	$7.8 \cdot 10^{-8}$	$1.6 \cdot 10^{-7}$	$1.7 \cdot 10^{-7}$	$2.5 \cdot 10^{-7}$	$3.7 \cdot 10^{-7}$
Lysogenic commitment time	h	13	183	352	376	558	807

[a]Abbreviations: Min, minimum; Qu, quartile; Max, maximum.

($1.7 \cdot 10^9$ cells/ml), duplication times (4.75 h), and volume of the human colon (400 ml [39]), we estimated that a median of $1.8 \cdot 10^{12}$ lysogens is potentially formed in the human gut every day via coinfection. Among marine communities, 90% displayed 10% or fewer bacteria becoming lysogens by coinfection (Fig. 4c, Table 2, and Table S1).

For communities with lysogeny above 1%, the most abundant phage-host pairs contributed an average of 67% ± 12% (standard deviation [SD]) for marine and 51% ± 16% for gut to the total lysogeny (Fig. 4d and Fig. S2). This was significantly higher than the contribution from the second most abundant phage-host pair, which yielded 13% ± 1% for marine and 15% ± 2% for gut. For communities with lysogeny above 1%, the most abundant phage-host rank displayed median COI of 1.00 (one infection on average) for marine (Fig. 4e, Fig. S2, and Table 3) and COI of 2.35 for gut (Fig. 4f, Fig. S2, and Table 4).

Physical parameters contributing to the formation of lysogens in communities. Communities with at least 1% lysogeny caused by coinfection were analyzed to extract the distribution of physical parameters yielding lysogeny. The distribution of bacterial abundances favoring lysogeny in marine communities was skewed toward high densities with a median of $1.5 \cdot 10^6$ cells/ml (Fig. 5a and Table 3). In gut communities, low bacterial abundances did not contribute to lysogeny, with the first quartile of the probability distribution at $9.2 \cdot 10^7$ cells/ml (Fig. 5a and Table 4). Phage concentrations yielding lysogeny in marine communities were also skewed toward higher densities (median of $9.1 \cdot 10^6$ phages/ml) but more centered than the bacterial density distribution (Fig. 5b and Table 3). In the gut, low phage concentrations did not contribute to lysogeny, displaying a first quartile of the probability distribution at $2.8 \cdot 10^8$ phages/ml (Fig. 5b and Table 4).

Phage adsorption rates in marine communities producing lysogeny were skewed toward high values with a median of $1.1 \cdot 10^{-7}$ ml/h (Fig. 5c and Table 3). In the gut, instead, the full range of adsorption rates contributed to communities with lysogeny (Fig. 5c and Table 4). The lysogenic commitment time in marine communities producing lysogeny was again skewed toward long time windows, with a median of 262 h (Fig. 5d and Table 3). For the gut, the full range of lysogenic commitment times contributed to producing lysogens, but larger values had a higher likelihood of contribution, displaying a median lysogenic commitment time of 0.92 h (Fig. 5d and Table 4).

DISCUSSION

The stochastic biophysical COI model introduced here estimated an increase in coinfections in the highly productive mammalian gut microbial communities (Fig. 4).

TABLE 3 Summary statistics for marine communities with lysogeny ≥1%[a]

Feature	Unit	Min	1st Qu	Median	Mean	3rd Qu	Max
Bacterial concentration	Cells/ml	$3.8 \cdot 10^4$	$4.7 \cdot 10^5$	$1.5 \cdot 10^6$	$2.1 \cdot 10^6$	$3.4 \cdot 10^6$	$6.7 \cdot 10^6$
Phage concentration	Phages/ml	$1.8 \cdot 10^5$	$4.0 \cdot 10^6$	$9.1 \cdot 10^6$	$1.3 \cdot 10^7$	$1.9 \cdot 10^7$	$3.9 \cdot 10^7$
Phage adsorption rate	ml/h	$1.4 \cdot 10^{-9}$	$4.6 \cdot 10^{-8}$	$1.1 \cdot 10^{-7}$	$1.4 \cdot 10^{-7}$	$2.1 \cdot 10^{-7}$	$3.7 \cdot 10^{-7}$
Lysogenic commitment time	h	11	109	262	311	489	807
Avg (co)infections (COI), rank 1	–	0.31	0.53	1.00	2.63	2.42	85.84
Avg (co)infections (COI), rank 2	–	0.19	0.33	0.62	1.64	1.51	53.43
Avg (co)infections (COI), rank 3	–	0.15	0.25	0.47	1.24	1.14	40.49

[a]Abbreviations: Min, minimum; Qu, quartile; Max, maximum; Avg, average; −, unitless.

TABLE 4 Summary statistics for gut communities with lysogeny ≥1%[a]

Feature	Unit	Min	1st Qu	Median	Mean	3rd Qu	Max
Bacterial concentration	Cells/ml	$3.8 \cdot 10^5$	$9.2 \cdot 10^7$	$4.4 \cdot 10^8$	$1.3 \cdot 10^9$	$1.9 \cdot 10^9$	$7.7 \cdot 10^9$
Phage concentration	Phages/ml	$3.1 \cdot 10^7$	$2.8 \cdot 10^8$	$5.3 \cdot 10^8$	$1.0 \cdot 10^9$	$1.2 \cdot 10^9$	$1.1 \cdot 10^{10}$
Phage adsorption rate	ml/h	$5.9 \cdot 10^{-8}$	$1.2 \cdot 10^{-7}$	$2.6 \cdot 10^{-7}$	$3.7 \cdot 10^{-7}$	$5.6 \cdot 10^{-7}$	$1.2 \cdot 10^{-6}$
Lysogenic commitment time	h	0.55	0.72	0.92	0.95	1.16	1.45
Avg (co)infections (COI), rank 1	–	0.33	0.88	2.35	7.29	7.19	182.07
Avg (co)infections (COI), rank 2	–	0.21	0.55	1.47	4.56	4.50	113.96
Avg (co)infections (COI), rank 3	–	0.16	0.42	1.12	3.47	3.42	86.64

[a]Abbreviations: Min, minimum; Qu, quartile; Max, maximum; Avg, average; −, unitless.

This higher frequency of coinfections predicts considerable levels of lysogeny in animal mucosa microbiomes, as observed empirically (9, 11, 12, 14, 16, 17), and supports the Piggyback-the-Winner framework (15, 16). In the murine gut, empirical genomic data show that 65.8% of the bacterial genomes are lysogens and that 83.2% of the prophages observed in these lysogens are active (40). Together, these lysogens reach relative abundances of 53.6% to 78.6% of the bacterial community. This frequency of lysogeny is consistent with the output of the coinfection model, which predicts lysogeny levels between 40% and 70% for abundances above 10^9 cells/ml (Fig. 4b, solid line). The model also predicted that 41.89% of the gut communities displaying lysogeny above 1% had virus-to-microbe ratios (VMR) lower than 1 (see Fig. S3 in the supplemental material), indicating that the formation of lysogens through coinfection was compatible with the observation of low virus-to-microbe ratios in high-density animal mucosa (12, 41). This was possible because coinfections were not required to occur

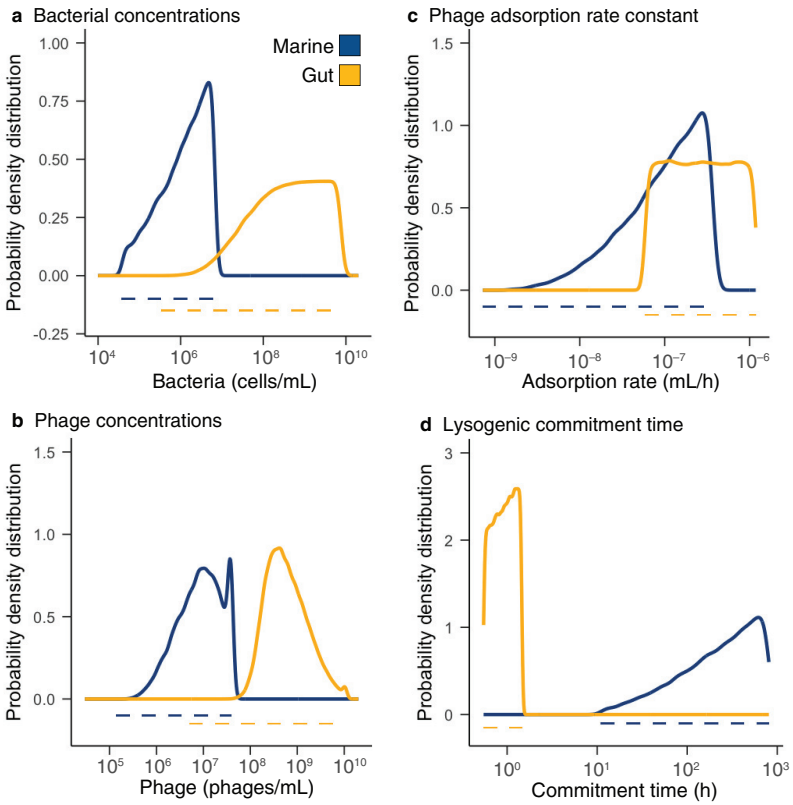

FIG 5 Ranges of parameter values leading to lysogeny caused by coinfection. Probability density distributions (solid lines) for bacterial abundances (a), phage concentrations (b), adsorption rates (c), and lysogenic commitment times (d) in marine (blue) and gut (yellow) communities displaying lysogeny levels above 1%. The dashed lines indicate the range of parameters explored in the model and obtained from the meta-analysis of each ecosystem. The probability densities were calculated with the logarithm in base 10 of the values displayed in the *x* axes.

simultaneously. Instead, they occurred within the lysogenic commitment time, which was assumed to be proportional to the duplication time of bacteria *in vivo* (42–44).

The lysogenic commitment time played a paramount role in the findings of the model because the duplication time of gut bacteria *in vivo* is significantly slower than the duplication time of gut bacterial isolates in pure cultures (42–44). For laboratory *E. coli* duplication times, the model predicted an average number of coinfections almost an order of magnitude lower than that *in vivo* (Fig. 1d). This result aligned with the low number of coinfections observed even at high MOIs in a recent stochastic model that used parameters similar to lambda and *E. coli* (38). The influence of the lysogenic commitment time was even more pronounced in marine communities (Fig. 5d). Lysogeny levels above 10% were favored for communities that displayed long lysogenic commitment times, which compensated for the lower adsorption rates and phage and bacterial abundances (Fig. 3 and 5).

The relationship between the lysogenic commitment time (τ) and duplication time in the biophysical COI model was based on lambda-*E. coli* single-cell experiments, which identified the relationship $\tau \sim$20% of the duplication time (25, 45). This pattern arises from the voting phenomenon, where each coinfecting phage genome independently votes for lytic or lysogenic commitment (46). In cells that undergo lysogeny, phages cooperate for host cell resources (25). Late phage genome arrivals contribute less to the cell-level decision, and the time window for the contribution of the second phage is proportional to the transcription level of phage repressors, which vary with the host growth rate (45). Future studies addressing the relationship between the lysogenic commitment time and host duplication time in other phages would refine the model and further test its validity in different ecosystems.

Only 10% of the simulated marine communities displayed levels of lysogeny above 10%. These communities were characterized by high phage and bacterial concentrations, displaying medians of $1.3 \cdot 10^7$ phages/ml and $2.0 \cdot 10^6$ cells/ml (Fig. 5a and b; Table 2). A direct comparison between empirical data and our model outputs was not possible due to the lack of estimates of percent lysogenic bacterial cells in marine environments using genomic data, which remains a bioinformatics challenge. Previous studies assessed the percentage of lysogeny in marine samples using mitomycin C induction, but this method has been proved inaccurate, and the density relationships derived from it are unclear (47). Alternatively, we pursued an indirect approach to compare the results of the model with empirical data by analyzing indicators of lysogeny that were available for both marine and gut ecosystems. In the free viral particle metagenomes, only 5% to 20% of the identified viral contigs are predicted to be temperate in marine samples (7), 3 to 15 times less than that observed in the gut, which ranges from 53% to 72% (40). When comparing genomes from isolates, marine bacteria encode 5 ± 2 (mean $\pm$ SD) prophages per genome, three times less than human gut bacteria, which encode 14 ± 5 prophages per genome (17). In the model, marine communities displayed, on average, 5 to 10 times less lysogeny than gut communities (solid lines in Fig. 4b). This ratio is on the same order of magnitude as the change in the two empirical indicators for lysogeny (temperate phage particles and prophage abundances) in marine and gut communities.

The stochastic community simulations assumed that the most dominant phages infected the most dominant bacteria (10, 11, 48–51). This empirically-based assumption allowed us to bridge the environmental data on viral and bacterial abundances with the species distributions from genomic data (Fig. 3). In the model, the most abundant phage-host pairs dominated the formation of lysogens (Fig. 4d and Fig. S2). If temperate phages do not occupy the first rank, lysogeny via coinfection will decrease by about 50% in marine and 70% in gut communities, unless there is a cross-infection network. Metagenomic data support that temperate phages and their hosts are likely to occupy high ranks in the community. For example, pelagiphages infecting SAR11, the most abundant marine bacterium, account for 35% of the phage particles in the virioplankton, representing the most abundant phages in the oceans, and 11 out of 16 isolated pelagiphages are temperate (50, 52, 53). If these closely related phages cooperate

during the lysogenic decision, their summed abundances would be much higher than the abundance of the highest rank in our model, 0.8% for marine communities. One challenge in building accurate phage-bacterial infection networks to test these comparisons is that the hosts of the majority of phages identified from metagenomic analyses are unknown (8, 54, 55). The reconstruction of accurate infection networks will, in the future, improve the model's predictive power on the contribution of coinfections to lysogeny (56, 57).

The average percentage of lysogens formed by coinfection decreased by almost 2 orders of magnitude as total bacterial concentrations dropped from 10^6 to 10^5 cells/ml (Fig. S1b). This contrasts with viral metagenomic studies from deep oceans with microbial abundances ranging from 10^4 to 10^5 cells/ml showing an increase in lysogeny compared to more productive surface waters (7, 20). In these environments, lysogeny has been proposed to serve as a low-density refugium for temperate phages in conditions of poor host growth and scarce resources for viral particle production (58–61). In the biophysical COI results, lysogeny in these low-cell-density communities occurred at very long commitment times (Fig. S4), which is likely the case in the natural environment. The model did not incorporate assumptions relating bacterial densities and commitment times. Adding this relationship would increase the percentage of lysogeny predicted in deep oligotrophic waters. Additional mechanisms could also contribute to the increase of lysogeny at these low concentrations, such as the favored phage integration in starved cells as observed in lambda due to the reduced degradation of the lytic repressor (62).

The COI model assumed that two phage infections occurring within the commitment time were necessary for lysogeny. This assumption was based on the observation that most temperate phages seem to encode a repressor system that is functionally similar to lambda's cro/cI (33, 34). This includes phages in marine environments, such as temperate phages infecting SAR11, suggesting that lessons learned from lambda can be extended to the marine environment (7, 52, 53). The model introduced here, however, does not capture lysogeny from a smaller fraction of temperate phages, such as P1 and P4-like, that do not respond to coinfections (63, 64). Further work will be necessary to assess alternative mechanisms for the control of lysogeny and refine the model predictions.

The lysogenic commitment time provides plasticity for phage adaptation to different ecosystems, which may be the reason why the response to coinfection has been selected in disparate environments. Phage densities are higher in the gut where bacterial replication times (and commitment times) are shorter than in marine environments. Above environment-specific density thresholds, communities would be driven to extinction by lysis unless immunity mechanisms emerge (65). Because of its superinfection immunity, lysogeny could be selected through the plastic coinfection response that depends on growth rates. Other density-dependent mechanisms, such as quorum sensing, may also contribute to maintaining population stability when phage densities are relatively high (66, 67). Coinfections might also act together with other molecular defenses, such as bacterial restriction-modification systems, which delay infection onset until bacteria reach densities that favor lysogeny via coinfection (68). Our model did not incorporate mechanisms that would lead to stability over long-term evolutionary dynamics (69). Further work will be necessary to assess these stability mechanisms.

Conclusion. The stochastic biophysical COI model proposed here identified the ranges of physical parameters that drive phage coinfections in complex microbial communities. The model predicted a high frequency of lysogeny caused by phage coinfections in the mammalian gut. This finding was a consequence of high phage and bacterial densities and high phage adsorption rates in comparison with marine communities. Longer lysogenic commitment times *in vivo*, compared to laboratory isolates, also contributed to high lysogeny in the gut. The simulated marine communities showed a lower frequency of lysogeny by coinfections. Those communities that displayed a high fraction of lysogeny were characterized by long lysogenic commitment times. Our findings

bridge the main molecular mechanism causing lysogeny in laboratory systems with metagenomic observations of lysogeny in complex microbial communities.

MATERIALS AND METHODS

Phage coinfection model. The average number of phage (co)infections (COI) was derived from physical properties of phage and bacteria (Fig. 1a). The rate of phage infections on a single bacterium can be estimated by solving the Smoluchowski coagulation equation (37). In a well-mixed community, this rate is the product of the phage concentration (P_i) and the phage adsorption rate (α), which depends on the mobilities and sizes of both the phage particle and the bacterium. The adsorption rate constant (α) expresses how fast a single phage adsorbs to a single bacterium given a volume (37), and its units are expressed here in ml/h. The subindex *i* specifies a single phage-bacterium pair in the community.

The number of (co)infections (COI) was defined as the number of phages infecting a cell within a given time window. This number was the product of the infection rate and the time window. In the case of lysogeny, this time corresponds to the lysogenic commitment time (τ), when the second phage can still interfere with the decision (lysis or lysogeny) of the first infecting phage (25). This led to the average phage coinfection equation (Fig. 1a)

$$\mathrm{COI} = \mathrm{P}_i \cdot \alpha \cdot \tau \tag{1}$$

Therefore, COI = 1 means one infection per cell on average within the window time, and COI = 2 means two phage infections. The average probability of coinfections was calculated assuming that each infection was independent and that, in a given environmental community, the changes in phage concentration (P_i) and bacterial concentrations (B_i) were small (within 20%) during the lysogenic commitment times (τ). This assumption is consistent with the typical changes of abundances in the environment (58, 70), but it does not apply during rapid changes in abundances observed under laboratory conditions (38). In the community model described below, the variance in COI due to the variance in (P_i) and (B_i) in a given community is negligible compared to the variance in COI resulting from the stochastic sampling across the ranges of microbial traits (see meta-analysis and stochastic sampling sections below).

The average number of coinfections was also expressed as a function of the phage-to-bacterium ratio, $\mathrm{COI} = \alpha \cdot \tau \cdot \mathrm{B}_i \cdot (\mathrm{P}_i/\mathrm{B}_i)$, as a proxy for comparison with lambda-to-*E. coli* ratio in MOI experiments. Numerically, the phage-to-bacterium ratio (P_i/B_i) was explored for the range 0.01 to 100. The median values extracted for the lambda adsorption rate ($\alpha_0 = 5.6 \cdot 10^{-7}$ ml/h), lysogenic commitment time ($\tau_0 =$ 0.1 h), and bacterial concentration ($B_0 = 5 \cdot 10^8$ cells/ml) were used as reference values (see section on meta-analysis for lambda parameters). Two parameters were fixed at these reference values, and the third was explored over a range of values based on the meta-analysis of microbial communities (see details below). These ranges were 10^5 to 10^{10} cells/ml for bacterial concentrations, 10^{-11} to 10^{-6} ml/h for the phage adsorption rates, and 10^{-3} to 10^2 h for the lysogenic commitment times.

Percentage of lysogeny for the coinfection model. A lysogen was formed when a cell was infected within the lysogenic commitment time by two or more phages from the same phage-host pair. This was based on the effect of cooperative infection by phages on the production of lysogens (24, 25, 46). Thus, the probability of lysogenization, p_{lys}, was determined by $p_{lys} = 1 - p(0) - p(1)$, where $p(k)$ was the probability of having k infections within the commitment time. The probability of k infections with average (co)infection COI, equation 1, was given by a Poisson distribution $p(k) = \mathrm{COI}^k \mathrm{e}^{-\mathrm{COI}}/k!$. The probability of forming a lysogen via coinfection was

$$p_{\mathrm{lys}} = 1 - \mathrm{e}^{-\mathrm{COI}} - \mathrm{COI}\,\mathrm{e}^{-\mathrm{COI}} \tag{2}$$

The model assumed that a higher probability of lysogenization resulted in a higher prevalence of lysogeny. This assumption was supported by experimental data (68, 69).

The probability of lysogenization was compared with the percentage of lysogeny obtained from lambda and *E. coli* MOI experiments (28, 29). The empirical data for the percentage of lysogeny and MOI were fitted using the nonlinear least-squares method for Hill-Langmuir cooperation models, $f(x) = ax/(b + x^n)$, with cooperation orders $n = 1$, $n = 2$, and $n = 3$.

Meta-analysis of marine and gut microbiomes. (i) Adsorption rates. The adsorption rates were obtained from 71 prior experiments using 19 phage-host pairs from marine and gut microbiomes (see Data Set S1 in the supplemental material). The data consisted of values for tailed phages infecting *E. coli* (37, 71), *Synechococcus* sp. (72–74), *Prochlorococcus* sp. (75–77), *Vibrio* sp. (78–81), *Roseobacter* sp. (82), and *Pseudoalteromonas* sp. (48). A *t* test (double-tailed) compared the marine and gut values.

(ii) Lysogenic commitment times. The lysogenic commitment time (τ) was assumed to be 20% of the bacterial duplication time (25, 45). The ranges of bacterial duplication times were obtained from *in situ* data sets for marine ecosystems (83) and from *in vivo* data sets for mammalian gut ecosystems (42–44) (Data Set S2).

(iii) VLPs and cell abundances. Direct counts of virus-like particles (VLPs) and microbial cells were obtained for marine surface waters (15, 84) and animal-associated microbiomes (41, 85–88) (Data Set S3). A *t* test (double-tailed) compared the concentrations of VLPs and cells between marine and animal ecosystems.

(iv) Phage and bacterial diversity. The rank-abundance curves of phage genotypes were constructed from the median slope and intercept of power-law functions fitted to 192 marine viromes and 1,158 human-associated viromes (89) (Data Set S4). Phage genotypes were defined as unique viral contigs at 98% sequence identity. The rank-abundance curves of bacterial species in marine communities were obtained from operational taxonomic unit (OTU) tables constructed by clustering universal, protein-coding, single-copy phylogenetic marker genes into metagenomic OTUs (which can be inter-

preted as species-level clusters) from the Tara Oceans data set (Data Set S5) (90, 91). For animal-associated bacterial microbiomes, rank-abundance curves were constructed using OTU tables obtained by mapping metagenomic reads from 11,850 human gut metagenomes to 92,143 metagenome-assembled genomes (92). Consensus rank-abundance curves were obtained by averaging the frequency of bacteria in the same rank across the metagenomes within each ecosystem.

Quantification of lysogeny through phage coinfection in communities. The biophysical COI model, equations 1 and 2, was applied to predict the probability of lysogenization in marine and gut ecosystems as a result of coinfection. The model generated stochastic communities that sampled empirical phage and bacterial concentrations, relative abundance of the top 100 members of the community, phage adsorption rates, and lysogenic commitment times obtained from the meta-analysis of marine and gut ecosystems described above.

(i) Stochastic sampling. The model generated 100,000 stochastic communities for both marine and gut ecosystems using Latin hypercube sampling (LHS). For each ecosystem, the ranges of bacterial concentrations, adsorption rates, and lysogenic commitment times were each divided into equal intervals in logarithmic scale (base 10), generating 100,000 points per coordinate. These coordinates defined the hypercube. One hundred thousand random values were sampled from the hypercube without repeating any coordinate value, that is, all coordinate values were sampled, following the standard LHS implementation (17, 93, 94).

(ii) Parameter ranges. The ranges of bacterial concentrations used were $3.78 \cdot 10^4$ to $6.75 \cdot 10^6$ bacteria/ml for marine communities and $3.45 \cdot 10^5$ to $7.60 \cdot 10^9$ bacteria/ml for gut. The ranges of phage concentrations used were $1.45 \cdot 10^5$ to $3.80 \cdot 10^7$ phages/ml for marine and $5.09 \cdot 10^6$ to $1.05 \cdot 10^{10}$ phages/ml for gut. The ranges of phage adsorption rate constants used were $7.2 \cdot 10^{-10}$ to $3.7 \cdot 10^{-7}$ ml/h for marine and $5.9 \cdot 10^{-8}$ to $1.2 \cdot 10^{-6}$ ml/h for gut. The ranges of lysogenic commitment times used were 11 h to 808 h for marine and 2.74 h to 7.27 h for gut. All parameter ranges were obtained in the meta-analysis described above.

(iii) Assumed relationships. Based on environmental data of microbial communities, the total phage concentration (P) was modeled following a power function relationship with the total bacterial concentration (B) (15, 17, 39, 95): $P(B) = a\ (B/B_u)^b$. The bacterial concentration was given in units of B_u = bacteria/ml. The prefactor a and exponent b were obtained by fitting the power function to the viral and microbial counts obtained in the marine and gut meta-analyses. A linear regression fit was applied using the least-squares method to the log-log data in base 10. The parameters obtained were $a = 10^{2.50}$ phage/ml and $b = 0.712$ for marine and $a = 10^{5.35}$ phage/ml and $b = 0.388$ for gut. To reproduce the noise observed in empirical communities, the value $\log_{10} P(B)$ was weighted by a normal distribution, N(mean, SD), with mean 1 and standard deviation 0.05 in logarithmic space (base 10), that is, $\log_{10}P = N(1,0.05) \cdot \log_{10}P(B)$. The final value of the phage concentration was constrained within the empirical phage abundance range, that is, $P_{min} \leq P \leq P_{max}$. The community model also assumed that the most dominant phages infected the most dominant bacteria (10, 11, 48–51). This led to a phage-host network where the phage of rank i infected the bacteria with the same rank i.

Data availability. The codes for the model are available in the GitHub repository at https://github.com/luque82/Luque_and_Silveira_2020.git.

SUPPLEMENTAL MATERIAL

Supplemental material is available online only.

FIG S1, EPS file, 1.9 MB.

FIG S2, EPS file, 1.9 MB.

FIG S3, EPS file, 1.5 MB.

FIG S4, JPG file, 0.1 MB.

TABLE S1, DOCX file, 0.01 MB.

DATA SET S1, CSV file, 0.003 MB.

DATA SET S2, CSV file, 0.01 MB.

DATA SET S3, CSV file, 0.1 MB.

DATA SET S4, CSV file, 0.02 MB.

DATA SET S5, CSV file, 0.002 MB.

ACKNOWLEDGMENTS

We thank Forest Rohwer, Anca Segall, Barbara Bailey, Peter Salamon, Rob Edwards, Elizabeth Dinsdale, and the SDSU Biomath Group for the discussions on phage coinfections and feedback on manuscript figures. We thank Kathryn Forcone for help obtaining data for meta-analysis and preparing figures.

REFERENCES

1. Touchon M, Bernheim A, Rocha EPC. 2016. Genetic and life-history traits associated with the distribution of prophages in bacteria. ISME J 10:2744–2754. https://doi.org/10.1038/ismej.2016.47.

2. Casjens S. 2003. Prophages and bacterial genomics: what have we learned so far? Mol Microbiol 49:277–300. https://doi.org/10.1046/j.1365-2958.2003.03580.x.

3. Fouts DE. 2006. Phage_Finder: automated identification and classification of prophage regions in complete bacterial genome sequences. Nucleic Acids Res 34:5839–5851. https://doi.org/10.1093/nar/gkl732.
4. Bondy-Denomy J, Qian J, Westra ER, Buckling A, Guttman DS, Davidson AR, Maxwell KL. 2016. Prophages mediate defense against phage infection through diverse mechanisms. ISME J 10:2854–2866. https://doi.org/10.1038/ismej.2016.79.
5. Mavrich TN, Hatfull GF. 2019. Evolution of superinfection immunity in cluster A mycobacteriophages. mBio 10:e00971-19. https://doi.org/10.1128/mBio.00971-19.
6. Jerlström Hultqvist J, Warsi O, Söderholm A, Knopp M, Eckhard U, Vorontsov E, Selmer M, Andersson DI. 2018. A bacteriophage enzyme induces bacterial metabolic perturbation that confers a novel promiscuous function. Nat Ecol Evol 2:1321–1330. https://doi.org/10.1038/s41559-018-0568-5.
7. Luo E, Eppley JM, Romano AE, Mende DR, DeLong EF. 2020. Double-stranded DNA virioplankton dynamics and reproductive strategies in the oligotrophic open ocean water column. ISME J 14:1304–1312. https://doi.org/10.1038/s41396-020-0604-8.
8. Silveira CB, Coutinho FH, Cavalcanti GS, Benler S, Doane MP, Dinsdale EA, Edwards RA, Francini-Filho RB, Thompson CC, Luque A, Rohwer FL, Thompson F. 2020. Genomic and ecological attributes of marine bacteriophages encoding bacterial virulence genes. BMC Genomics 21:126. https://doi.org/10.1186/s12864-020-6523-2.
9. Reyes A, Haynes M, Hanson N, Angly FE, Heath AC, Rohwer F, Gordon JI. 2010. Viruses in the faecal microbiota of monozygotic twins and their mothers. Nature 466:334–338. https://doi.org/10.1038/nature09199.
10. Minot S, Sinha R, Chen J, Li H, Keilbaugh SA, Wu GD, Lewis JD, Bushman FD. 2011. The human gut virome: inter-individual variation and dynamic response to diet. Genome Res 21:1616–1625. https://doi.org/10.1101/gr.122705.111.
11. Minot S, Bryson A, Chehoud C, Wu GD, Lewis JD, Bushman FD. 2013. Rapid evolution of the human gut virome. Proc Natl Acad Sci U S A 110:12450–12455. https://doi.org/10.1073/pnas.1300833110.
12. Mirzaei M, Khan MAA, Ghosh P, Taranu ZE, Taguer M, Ru J, Chowdhury R, Kabir MM, Deng L, Mondal D, Maurice CF. 2020. Bacteriophages isolated from stunted children can regulate gut bacterial communities in an age-specific manner. Cell Host Microbe 27:199–212.e5. https://doi.org/10.1016/j.chom.2020.01.004.
13. Beller L, Matthijnssens J. 2019. What is (not) known about the dynamics of the human gut virome in health and disease. Curr Opin Virol 37:52–57. https://doi.org/10.1016/j.coviro.2019.05.013.
14. Shkoporov AN, Hill C. 2019. Bacteriophages of the human gut: the "known unknown" of the microbiome. Cell Host Microbe 25:195–209. https://doi.org/10.1016/j.chom.2019.01.017.
15. Knowles B, Silveira CB, Bailey BA, Barott K, Cantu VA, Cobián-Güemes A, Coutinho FH, Dinsdale EA, Felts B, Furby KA, George EE, Green KT, Gregoracci GB, Haas AF, Haggerty JM, Hester ER, Hisakawa N, Kelly LW, Lim YW, Little M, Luque A, McDole-Somera T, McNair K, de Oliveira LS, Quistad SD, Robinett NL, Sala E, Salamon P, Sanchez SE, Sandin S, Silva GGZ, Smith J, Sullivan C, Thompson C, Vermeij MJA, Youle M, Young C, Zgliczynski B, Brainard R, Edwards RA, Nulton J, Thompson F, Rohwer F. 2016. Lytic to temperate switching of viral communities. Nature 531:466–470. https://doi.org/10.1038/nature17193.
16. Silveira CB, Rohwer FL. 2016. Piggyback-the-Winner in host-associated microbial communities. NPJ Biofilms Microbiomes 2:16010. https://doi.org/10.1038/npjbiofilms.2016.10.
17. Anthenelli M, Jasien E, Edwards R, Bailey B, Felts B, Katira P, Nulton J, Salamon P, Rohwer F, Silveira CB, Luque A. 2020. Phage and bacteria diversification through a prophage acquisition ratchet. bioRxiv https://doi.org/10.1101/2020.04.08.028340.
18. Muck S, Griessler T, Köstner N, Klimiuk A, Winter C, Herndl GJ. 2014. Fracture zones in the Mid Atlantic Ridge lead to alterations in prokaryotic and viral parameters in deep-water masses. Front Microbiol 5:264. https://doi.org/10.3389/fmicb.2014.00264.
19. Luo E, Aylward FO, Mende DR, DeLong EF. 2017. Bacteriophage distributions and temporal variability in the ocean's interior. mBio 8:e01903-17. https://doi.org/10.1128/mBio.01903-17.
20. Coutinho FH, Rosselli R, Rodríguez-Valera F. 2019. Trends of microdiversity reveal depth-dependent evolutionary strategies of viruses in the Mediterranean. mSystems 4:e00554-19. https://doi.org/10.1128/mSystems.00554-19.
21. Paul JH. 2008. Prophages in marine bacteria: dangerous molecular time bombs or the key to survival in the seas? ISME J 2:579–589. https://doi.org/10.1038/ismej.2008.35.
22. Lauro FM, McDougald D, Thomas T, Williams TJ, Egan S, Rice S, DeMaere MZ, Ting L, Ertan H, Johnson J, Ferriera S, Lapidus A, Anderson I, Kyrpides N, Munk AC, Detter C, Han CS, Brown MV, Robb FT, Kjelleberg S, Cavicchioli R. 2009. The genomic basis of trophic strategy in marine bacteria. Proc Natl Acad Sci U S A 106:15527–15533. https://doi.org/10.1073/pnas.0903507106.
23. Oppenheim AB, Kobiler O, Stavans J, Court DL, Adhya S. 2005. Switches in bacteriophage lambda development. Annu Rev Genet 39:409–429. https://doi.org/10.1146/annurev.genet.39.073003.113656.
24. Golding I. 2016. Single-cell studies of phage λ: hidden treasures under Occam's rug. Annu Rev Virol 3:453–472. https://doi.org/10.1146/annurev-virology-110615-042127.
25. Trinh JT, Székely T, Shao Q, Balázsi G, Zeng L. 2017. Cell fate decisions emerge as phages cooperate or compete inside their host. Nat Commun 8:14341. https://doi.org/10.1038/ncomms14341.
26. Boyd JSK. 1951. Observations on the relationship of symbiotic and lytic bacteriophage. J Pathol Bacteriol 63:445–457. https://doi.org/10.1002/path.1700630311.
27. Lieb M. 1953. The establishment of lysogenicity in *Escherichia coli*. J Bacteriol 65:642–651. https://doi.org/10.1128/JB.65.6.642-651.1953.
28. Fry BA. 1959. Conditions for the infection of *Escherichia coli* with lambda phage and for the establishment of lysogeny. J Gen Microbiol 21:676–684. https://doi.org/10.1099/00221287-21-3-676.
29. Kourilsky P. 1973. Lysogenization by bacteriophage lambda. Mol Gen Genet 122:183–195. https://doi.org/10.1007/BF00435190.
30. Herskowitz I, Hagen D. 1980. The lysis-lysogeny decision of phage lambda: explicit programming and responsiveness. Annu Rev Genet 14:399–445. https://doi.org/10.1146/annurev.ge.14.120180.002151.
31. Kourilsky P. 1975. Lysogenization by bacteriophage lambda. II. Identification of genes involved in the multiplicity dependent processes. Biochimie 56:1511–1516. https://doi.org/10.1016/S0300-9084(75)80274-4.
32. Cheng HH, Muhlrad PJ, Hoyt MA, Echols H. 1988. Cleavage of the cII protein of phage lambda by purified HflA protease: control of the switch between lysis and lysogeny. Proc Natl Acad Sci U S A 85:7882–7886. https://doi.org/10.1073/pnas.85.21.7882.
33. Ptashne M. 1986. A genetic switch: gene control and phage lambda. Cell Press, Cambridge, MA.
34. Golding I, Coleman S, Nguyen TVP, Yao T. 2019. Decision making by temperate phages. *In* Reference module in life sciences. Elsevier, New York, NY.
35. Whipple FW, Kuldell NH, Cheatham LA, Hochschild A. 1994. Specificity determinants for the interaction of lambda repressor and P22 repressor dimers. Genes Dev 8:1212–1223. https://doi.org/10.1101/gad.8.10.1212.
36. Bourret RB, Fox MS. 1988. Lysogenization of Escherichia coli him+, himA, and himD hosts by bacteriophage Mu. J Bacteriol 170:1672–1682. https://doi.org/10.1128/jb.170.4.1672-1682.1988.
37. Joiner KL, Baljon A, Barr J, Rohwer F, Luque A. 2019. Impact of bacteria motility in the encounter rates with bacteriophage in mucus. Sci Rep 9:16427. https://doi.org/10.1038/s41598-019-52794-2.
38. Lang M, Pleška M, Guet CC. 2020. Population dynamics of decision making in temperate bacteriophages. bioRxiv https://doi.org/10.1101/2020.03.18.996918.
39. Parikka KJ, Le Romancer M, Wauters N, Jacquet S. 2017. Deciphering the virus-to-prokaryote ratio (VPR): insights into virus-host relationships in a variety of ecosystems. Biol Rev 92:1081–1100. https://doi.org/10.1111/brv.12271.
40. Kim M-S, Bae J-W. 2018. Lysogeny is prevalent and widely distributed in the murine gut microbiota. ISME J 12:1127–1141. https://doi.org/10.1038/s41396-018-0061-9.
41. Kim M-S, Park E-J, Roh SW, Bae J-W. 2011. Diversity and abundance of single-stranded DNA viruses in human feces. Appl Environ Microbiol 77:8062–8070. https://doi.org/10.1128/AEM.06331-11.
42. Vandeputte D, Falony G, Vieira-Silva S, Tito RY, Joossens M, Raes J. 2016. Stool consistency is strongly associated with gut microbiota richness and composition, enterotypes and bacterial growth rates. Gut 65:57–62. https://doi.org/10.1136/gutjnl-2015-309618.
43. Heinken A, Sahoo S, Fleming RMT, Thiele I. 2013. Systems-level characterization of a host-microbe metabolic symbiosis in the mammalian gut. Gut Microbes 4:28–40. https://doi.org/10.4161/gmic.22370.
44. Myhrvold C, Kotula JW, Hicks WM, Conway NJ, Silver PA. 2015. A distributed

cell division counter reveals growth dynamics in the gut microbiota. Nat Commun 6:10039–10010. https://doi.org/10.1038/ncomms10039.
45. Cortes MG, Trinh JT, Zeng L, Balázsi G. 2017. Late-arriving signals contribute less to cell-fate decisions. Biophys J 113:2110–2120. https://doi.org/10.1016/j.bpj.2017.09.012.
46. Zeng L, Skinner SO, Zong C, Sippy J, Feiss M, Golding I. 2010. Decision making at a subcellular level determines the outcome of bacteriophage infection. Cell 141:682–691. https://doi.org/10.1016/j.cell.2010.03.034.
47. Knowles B, Bailey B, Boling L, Breitbart M, Cobián-Güemes A, Del Campo J, Edwards R, Felts B, Grasis J, Haas AFAF, Katira P, Kelly LWLW, Luque A, Nulton J, Paul L, Peters G, Robinett N, Sandin S, Segall A, Silveira C, Youle M, Rohwer F. 2017. Variability and host density independence in inductions-based estimates of environmental lysogeny. Nat Microbiol 2:17064. https://doi.org/10.1038/nmicrobiol.2017.64.
48. Deng L, Gregory A, Yilmaz S, Poulos BT, Hugenholtz P, Sullivan MB. 2013. Contrasting life strategies of viruses that infect photo- and heterotrophic bacteria, as revealed by viral tagging. mBio 4:e00516-12. https://doi.org/10.1128/mBio.00516-12.
49. Coutinho FH, Silveira CB, Gregoracci GB, Thompson CC, Edwards RA, Brussaard CP, Dutilh BE, Thompson FL. 2017. Marine viruses discovered via metagenomics shed light on viral strategies throughout the oceans. Nat Commun 8:15955. https://doi.org/10.1038/ncomms15955.
50. Zhao Y, Temperton B, Thrash JC, Schwalbach MS, Vergin KL, Landry ZC, Ellisman M, Deerinck T, Sullivan MB, Giovannoni SJ. 2013. Abundant SAR11 viruses in the ocean. Nature 494:357–360. https://doi.org/10.1038/nature11921.
51. Džunková M, Low SJ, Daly JN, Deng L, Rinke C, Hugenholtz P. 2019. Defining the human gut host–phage network through single-cell viral tagging. Nat Microbiol 4:2192–2203. https://doi.org/10.1038/s41564-019-0526-2.
52. Morris RM, Cain KR, Hvorecny KL, Kollman JM. 2020. Lysogenic host–virus interactions in SAR11 marine bacteria. Nat Microbiol 5:1011–1015. https://doi.org/10.1038/s41564-020-0725-x.
53. Zhao Y, Qin F, Zhang R, Giovannoni SJ, Zhang Z, Sun J, Du S, Rensing C. 2019. Pelagiphages in the Podoviridae family integrate into host genomes. Environ Microbiol 21:1989–2001. https://doi.org/10.1111/1462-2920.14487.
54. Edwards RA, McNair K, Faust K, Raes J, Dutilh BE. 2016. Computational approaches to predict bacteriophage–host relationships. FEMS Microbiol Rev 40:258–272. https://doi.org/10.1093/femsre/fuv048.
55. Gregory AC, Zayed AA, Conceição-Neto N, Temperton B, Bolduc B, Alberti A, Ardyna M, Arkhipova K, Carmichael M, Cruaud C, Dimier C, Domínguez-Huerta G, Ferland J, Kandels S, Liu Y, Marec C, Pesant S, Picheral M, Pisarev S, Poulain J, Tremblay JÉ, Vik D, Acinas SG, Babin M, Bork P, Boss E, Bowler C, Cochrane G, de Vargas C, Follows M, Gorsky G, Grimsley N, Guidi L, Hingamp P, Iudicone D, Jaillon O, Kandels-Lewis S, Karp-Boss L, Karsenti E, Not F, Ogata H, Poulton N, Raes J, Sardet C, Speich S, Stemmann L, Sullivan MB, Sunagawa S, Wincker P, Culley AI, Dutilh BE, Roux S, Tara Oceans Coordinators. 2019. Marine DNA viral macro- and microdiversity from pole to pole. Cell 177:1109–1123.e14. https://doi.org/10.1016/j.cell.2019.03.040.
56. Marbouty M, Baudry L, Cournac A, Koszul R. 2017. Scaffolding bacterial genomes and probing host-virus interactions in gut microbiome by proximity ligation (chromosome capture) assay. Sci Adv 3:e1602105. https://doi.org/10.1126/sciadv.1602105.
57. Labonté JM, Swan BK, Poulos B, Luo H, Koren S, Hallam SJ, Sullivan MB, Woyke T, Wommack KE, Stepanauskas R. 2015. Single-cell genomics-based analysis of virus–host interactions in marine surface bacterioplankton. ISME J 9:2386–2399. https://doi.org/10.1038/ismej.2015.48.
58. Brum JR, Hurwitz BL, Schofield O, Ducklow HW, Sullivan MB. 2016. Seasonal time bombs: dominant temperate viruses affect Southern Ocean microbial dynamics. ISME J 10:437–449. https://doi.org/10.1038/ismej.2015.125.
59. Paul JH, Weinbauer M. 2010. Detection of lysogeny in marine environments, p 30–33. *In* Wilhelm SW, Weinbauer MG, Suttle CA (ed), Manual of aquatic viral ecology. American Society of Limnology and Oceanography, Waco, TX.
60. Jiang SC, Paul JH. 1994. Seasonal and diel abundance of viruses and occurrence of lysogeny/bacteriocinogeny in the marine environment. Mar Ecol Prog Ser 104:163–172. https://doi.org/10.3354/meps104163.
61. Maurice CF, Bouvier T, Comte J, Guillemette F, Del Giorgio PA. 2010. Seasonal variations of phage life strategies and bacterial physiological states in three northern temperate lakes. Environ Microbiol 12:628–641. https://doi.org/10.1111/j.1462-2920.2009.02103.x.
62. Shotland Y, Koby S, Teff D, Mansur N, Oren DA, Tatematsu K, Tomoyasu T, Kessel M, Bukau B, Ogura T, Oppenheim AB. 1997. Proteolysis of the phage lambda CII regulatory protein by FtsH (HflB) of Escherichia coli. Mol Microbiol 24:1303–1310. https://doi.org/10.1046/j.1365-2958.1997.4231796.x.
63. Rosner JL. 1972. Formation, induction, and curing of bacteriophage P1 lysogens. Virology 48:679–689. https://doi.org/10.1016/0042-6822(72)90152-3.
64. Christie GE, Calendar R. 1990. Interactions between satellite bacteriophage P4 and its helpers. Annu Rev Genet 24:465–490. https://doi.org/10.1146/annurev.ge.24.120190.002341.
65. Xue C, Goldenfeld N. 2017. Coevolution maintains diversity in the stochastic "Kill the Winner" model. Phys Rev Lett 119:268101. https://doi.org/10.1103/PhysRevLett.119.268101.
66. Erez Z, Steinberger-Levy I, Shamir M, Doron S, Stokar-Avihail A, Peleg Y, Melamed S, Leavitt A, Savidor A, Albeck S, Amitai G, Sorek R. 2017. Communication between viruses guides lysis–lysogeny decisions. Nature 541:488–493. https://doi.org/10.1038/nature21049.
67. Tan D, Hansen MF, de Carvalho LN, Røder HL, Burmølle M, Middelboe M, Svenningsen SL. 2020. High cell densities favor lysogeny: induction of an H20 prophage is repressed by quorum sensing and enhances biofilm formation in Vibrio anguillarum. ISME J 14:1731–1712. https://doi.org/10.1038/s41396-020-0641-3.
68. Pleška M, Lang M, Refardt D, Levin BR, Guet CC. 2018. Phage–host population dynamics promotes prophage acquisition in bacteria with innate immunity. Nat Ecol Evol 2:359–366. https://doi.org/10.1038/s41559-017-0424-z.
69. Chaudhry W, Vega N, Govindan AR, Garcia R, Lee E, McCall IC, Levin BR. 2019. The population and evolutionary dynamics of bacteriophage: why be temperate revisited. bioRxiv https://doi.org/10.1101/824235.
70. Silveira CB, Gregoracci GB, Coutinho FH, Soares AC, Silva GGZ, Haggerty JM, Oliveira LS, Francini-Filho RB, Edwards RA, Dinsdale EA, Thompson CC, Thompson FL. 2017. Bacterial community associated with the reef coral *Mussismilia braziliensis*'s boundary layer over a diel cycle. Front Microbiol 8:784. https://doi.org/10.3389/fmicb.2017.00784.
71. Schwartz M. 1976. The adsorption of coliphage lambda to its host: effect of variations in the surface density of receptor and in phage-receptor affinity. J Mol Biol 103:521–536. https://doi.org/10.1016/0022-2836(76)90215-1.
72. Waterbury JB, Valois FW. 1993. Resistance to co-occurring phages enables marine Synechococcus communities to coexist with cyanophages abundant in seawater. Appl Environ Microbiol 59:3393–3399. https://doi.org/10.1128/AEM.59.10.3393-3399.1993.
73. Mann NH. 2003. Phages of the marine cyanobacterial picophytoplankton. FEMS Microbiol Rev 27:17–34. https://doi.org/10.1016/S0168-6445(03)00016-0.
74. Stoddard LI, Martiny JBH, Marston MF. 2007. Selection and characterization of cyanophage resistance in marine Synechococcus strains. Appl Environ Microbiol 73:5516–5522. https://doi.org/10.1128/AEM.00356-07.
75. Avrani S, Wurtzel O, Sharon I, Sorek R, Lindell D. 2011. Genomic island variability facilitates Prochlorococcusvirus coexistence. Nature 474:604–608. https://doi.org/10.1038/nature10172.
76. Schwartz DA, Lindell D. 2017. Genetic hurdles limit the arms race between Prochlorococcus and the T7-like podoviruses infecting them. ISME J 11:1836–1851. https://doi.org/10.1038/ismej.2017.47.
77. Beckett SJ, Demory D, Coenen AR, Casey JR, Follett CL, Dugenne M, Connell PE, Carlson MCG, Hu SK, Wilson ST. 2019. A day in the life of Prochlorococcus: diel ecological oscillations of cyanobacteria, viruses and grazers in the North Pacific Subtropical Gyre. 2019 ESA Annual Meeting (August 11–16). Ecological Society of America, Washington, DC.
78. Levisohn R, Moreland J, Nealson KH. 1987. Isolation and characterization of a generalized transducing phage for the marine luminous bacterium Vibrio fischeri MJ-1. J Gen Microbiol 133:1577–1582. https://doi.org/10.1099/00221287-133-6-1577.
79. Johnson RM. 1968. Characteristics of a marine Vibrio-bacteriophage system. J Ariz Acad Sci 5:28–33. https://doi.org/10.2307/40022820.
80. Cohen Y, Pollock FJ, Rosenberg E, Bourne DG. 2013. Phage therapy treatment of the coral pathogen Vibrio coralliilyticus. Microbiologyopen 2:64–74. https://doi.org/10.1002/mbo3.52.
81. Castillo D, Alvise PD, Xu R, Zhang F, Middelboe M, Gram L. 2017. Comparative genome analyses of Vibrio anguillarum strains reveal a link with pathogenicity traits. mSystems 2:e00001-17. https://doi.org/10.1128/mSystems.00001-17.
82. Huang C, Zhang Y, Jiao N. 2010. Phage resistance of a marine bacterium,

Roseobacter denitrificans OCh114, as revealed by comparative proteomics. Curr Microbiol 61:141–147. https://doi.org/10.1007/s00284-010-9588-3.
83. Kirchman DL. 2016. Growth rates of microbes in the oceans. Annu Rev Mar Sci 8:285–309. https://doi.org/10.1146/annurev-marine-122414-033938.
84. Parsons RJ, Breitbart M, Lomas MW, Carlson CA. 2012. Ocean time-series reveals recurring seasonal patterns of virioplankton dynamics in the northwestern Sargasso Sea. ISME J 6:273–284. https://doi.org/10.1038/ismej.2011.101.
85. Barr JJ, Auro R, Furlan M, Whiteson KL, Erb ML, Pogliano J, Stotland A, Wolkowicz R, Cutting AS, Doran KS, Salamon P, Youle M, Rohwer F. 2013. Bacteriophage adhering to mucus provide a non–host-derived immunity. Proc Natl Acad Sci U S A 110:10771–10776. https://doi.org/10.1073/pnas.1305923110.
86. Furlan M. 2009. Viral and microbial dynamics in the human respiratory tract. San Diego State University, San Diego, CA.
87. Hoyles L, Honda H, Logan NA, Halket G, La Ragione RM, McCartney AL. 2008. Isolation of Bacillus clausii, Bacillus licheniformis and other bacilli from human faecal samples. INRA–Rowett 2008 Gut Microbiome Funct Interact Host Impact Environ.
88. Lepage P, Colombet J, Marteau P, Sime-Ngando T, Doré J, Leclerc M. 2008. Dysbiosis in inflammatory bowel disease: a role for bacteriophages? Gut 57:424–425. https://doi.org/10.1136/gut.2007.134668.
89. Cobián Güemes AG, Youle M, Cantú VA, Felts B, Nulton J, Rohwer F. 2016. Viruses as winners in the game of life. Annu Rev Virol 3:197–214. https://doi.org/10.1146/annurev-virology-100114-054952.
90. Sunagawa S, Mende DR, Zeller G, Izquierdo-Carrasco F, Berger SA, Kultima JR, Coelho LP, Arumugam M, Tap J, Nielsen HB, Rasmussen S, Brunak S, Pedersen O, Guarner F, De Vos WM, Wang J, Li J, Doré J, Dusko Ehrlich S, Stamatakis A, Bork P. 2013. Metagenomic species profiling using universal phylogenetic marker genes. Nat Methods 10:1196–1199. https://doi.org/10.1038/nmeth.2693.
91. Mende DR, Sunagawa S, Zeller G, Bork P. 2013. Accurate and universal delineation of prokaryotic species. Nat Methods 10:881–884. https://doi.org/10.1038/nmeth.2575.
92. Almeida A, Mitchell AL, Boland M, Forster SC, Gloor GB, Tarkowska A, Lawley TD, Finn RD. 2019. A new genomic blueprint of the human gut microbiota. Nature 568:499–504. https://doi.org/10.1038/s41586-019-0965-1.
93. Weitz JS, Beckett SJ, Brum JR, Cael BB, Dushoff J. 2017. Lysis, lysogeny and virus–microbe ratios. Nature 549:E1–E3. https://doi.org/10.1038/nature23295.
94. McKay MD, Beckman RJ, Conover WJ. 1979. Comparison of three methods for selecting values of input variables in the analysis of output from a computer code. Technometrics 21:239–245. https://doi.org/10.2307/1268522.
95. Wigington CH, Sonderegger D, Brussaard CPD, Buchan A, Finke JF, Fuhrman JA, Lennon JT, Middelboe M, Suttle CA, Stock C, Wilson WH, Wommack KE, Wilhelm SW, Weitz JS. 2016. Re-examination of the relationship between marine virus and microbial cell abundances. Nat Microbiol 1:15024. https://doi.org/10.1038/nmicrobiol.2015.24.